Numerical simulation of the power dissipated by the aerodynamics of a prototype mobile electric generator

Sidy Mactar SOKHNA[1], Mohamed El Amine AIT ALI[2], Souleye FAYE[1], Vincent SAMBOU[1], and Mohamed AGOUZOUL[2]

[1]Laboratoire Eau-Energie-Environnement et Procédés Industriels, Université Cheikh Anta DIOP, Ecole Supérieure Polytechnique, Fann, Dakar, Senegal

[2]Équipe de Recherche Génie Mécanique et Énergétique: Modélisation et Expérimentation ERG2 (ME), Université Mohammed V de Rabat, Ecole Mohammadia d'Ingénieurs, Rabat-Agdal, Rabat, Morocco

---

ABSTRACT: The article investigates power losses caused by aerodynamic forces in a stand-alone photovoltaic generator. The generator is designed to meet electrical energy requirements and is propelled by 3000 W electric motors in the rear wheels. To overcome resistances, including the variable air resistance at different speeds, the propulsion system is utilized. Numerical methods are employed to investigate the interplay between structure, shape, and performance. The contrast in pressure between the front and back of the generator creates a significant amount of pressure, mostly caused by aerodynamic drag. This occurrence is dictated by the body's shape being examined concerning the airflow while in motion at a designated velocity, ascertaining the air's force and dynamic pressure. During changes in speed, power is dissipated. The purpose of this study is to determine the value of this power. Numerical and analytical models provide results for this physical phenomenon. The findings of numerical simulations, which used ANSYS 2020 R1 and SolidWorks 2020 SP5 software, concerning the airflow over the generator are presented. The numerical and analytical methods show only a slight difference; 4.22% for drag force and 6.10% for dynamic pressure. These results indicate energy losses due to air resistance, revealing that a speed increase of 3 km/h results in a power decrease of 12.69 W, with rolling resistance being taken into account. It is worth noting that the total power lost amounts to 1438.55 W.

KEYWORDS: Aerodynamic, Drag; Dissipated Power, Electrical generator Photovoltaic, Resistance to movement.

1   INTRODUCTION

The situation is alarming: emissions from fossil-fuel vehicles continue to increase yearly, causing a harmful impact on the planet. To combat global warming, there is a need to improve vehicle performance by reducing energy consumption and increasing range. Some manufacturers are already transitioning towards electric vehicles [1] due to the advancements in technology and promotion. Reducing rolling resistance, mass employing lightweight materials, and optimizing aerodynamics are key factors that affect vehicle characteristics, including fuel consumption, top speed, and braking [2]. To enhance vehicle autonomy and performance, numerous technologies [3] have been developed.

Power is directly proportional to the coefficient of drag, which is responsible for a significant portion of power dissipation [4]. Moreover, handling is an essential safety concern [5], and wind flow has a significant impact on the handling components. During the 1930s, manufacturers spent a considerable amount of time studying drag while in motion. Therefore, driving conditions varied across different regions, depending on the wind and shape [6]. In the 1950s, researchers, such as Riedler, conceptualized aerodynamic shape. This involved evaluating various forms of resistance encountered during travel, including air resistance, slope resistance and rolling resistance [7].

Aerodynamics generates several forces on a body and particularly on a vehicle in motion [8] At a given maximum speed, it becomes more important and has an impact on the power of the engine, whether for an internal combustion engine or an

---

electric motor. In the case of combustion engines, at 70 km/h, aerodynamics is the primary source of fuel consumption [9]. The phenomena related to the fluid dynamics of a vehicle are studied for power optimization, hence the importance of studying the aerodynamics of the generator. The power used to overcome air resistance depends on the speed of the vehicle.

The vehicle produces electrical energy and uses the energy it generates to move around. The battery voltage measured was 51.3 V, made up of 16 cells each producing 3.2 V. In addition, the average daily solar irradiation is 481 W/m2, and the measurements were taken at an ambient temperature of 27°C. The BLDC wheel motors have a rated power of 3000 V. The motor current is 8 A. It has 9 speeds.

As the vehicle is powered entirely by photovoltaic cells and is the first of its kind to be built in Senegal, it is essential to characterise it using this specific data. The data assembled will permit us to observe the impact of air resistance on the electric vehicle under trial conditions in the Sahel region.

Air resistance affects the generator and impacts its range. It diminishes its power by drawing some of it to move the air masses around the vehicle. The aim of this research is to investigate the effect of aerodynamics on power dissipation, focusing on a limited scope. To achieve our objective, we will compare numerical and analytical calculations, along with a numerical simulation to describe how aerodynamics affects the electric generator's power output at various speeds [10]. It is worth noting that aerodynamics plays a defining role in determining the maximum speed of the vehicle [11], as such, we will investigate the aerodynamic behavior of the generator at top speed [12].

2 FACTORS INFLUENCING AERODYNAMICS

When an object moves, it encounters the surrounding air, which creates forces around the object [13]. The total effect of these forces acting on the object's shape is known as the aerodynamic body. Consequently, the air imposes both frictional and pressure forces on the object. The speed determines the force acting on the body, causing the generation of a moment related to the dynamic air pressure and characteristic lengths [12]. To achieve optimal performance, the drag of a car designed for solar power must be kept to a minimum [14].

The equations (1) and (2) provide the values for the force and moment.

$$F_a = F_{xi} + F_{yi} + F_{zi} \quad (1)$$

$$M_a = M_{xi} + M_{yi} + M_{zi} \quad (2)$$

2.1 DRAG COEFFICIENT

The drag coefficient [15] is defined as the ratio of the drag force of the aerodynamic torsor on the axis of the direction of motion to the dynamic pressure relative to the speed of motion on the frontal surface, which is the surface whose direction of motion is normal to it [16].

$$C_x = \frac{R_a}{\frac{1}{2} \times \alpha \times S \times v^2} \quad (3)$$

Some perspectives [17] define drag as the force that opposes the motion of an object through a fluid. The drag coefficient relies on the speed of the flow [18], but it only slightly fluctuates in specific speed ranges [19]. Typically, a vehicle experiences minor variation in the drag coefficient between 90 and 130 km/h [20].

Drag affects a vehicle in four ways:

- Shape drags: the result of a shape's frontal impact;
- Vortex drag: due to the vortices that form around a shape;
- Surface drag: caused by the air friction against the bodywork;
- Internal drag: arising from the air resistance as it flows through the vehicle.

Shape			Drag Coefficient Cx
Sphere			0.47
Streamline body			0.04
Cube			1.13
Hollow hemispher			0.42
Cylinder			1.15
Long Cylinder			0.82
Angled Cube			0.8

Fig. 1.   Frontal Drag coefficient [24]

The drag coefficients following the torsor are given by the following equations:

F x: Drag

$$Cx = \frac{R_a}{\frac{1}{2} \times \alpha \times S \times v^2} \qquad (4)$$

M x: Roll

$$C_r = \frac{M_X}{\frac{1}{2} \times \alpha \times S \times v^2 \times La} \qquad (5)$$

F y: Drift

$$C_d = \frac{Fy}{\frac{1}{2} \times \alpha \times S \times v^2} \qquad (6)$$

M y: Pitch

$$C_t = \frac{M_Y}{\frac{1}{2} \times \alpha \times S \times v^2 \times La} \qquad (7)$$

F z: lift

$$C_p = \frac{F_z}{\frac{1}{2} \times \alpha \times S \times v^2} \qquad (8)$$

M z: Lacet

$$C_l = \frac{M_Z}{\frac{1}{2} \times \alpha \times S \times v^2 \times La} \qquad (9)$$
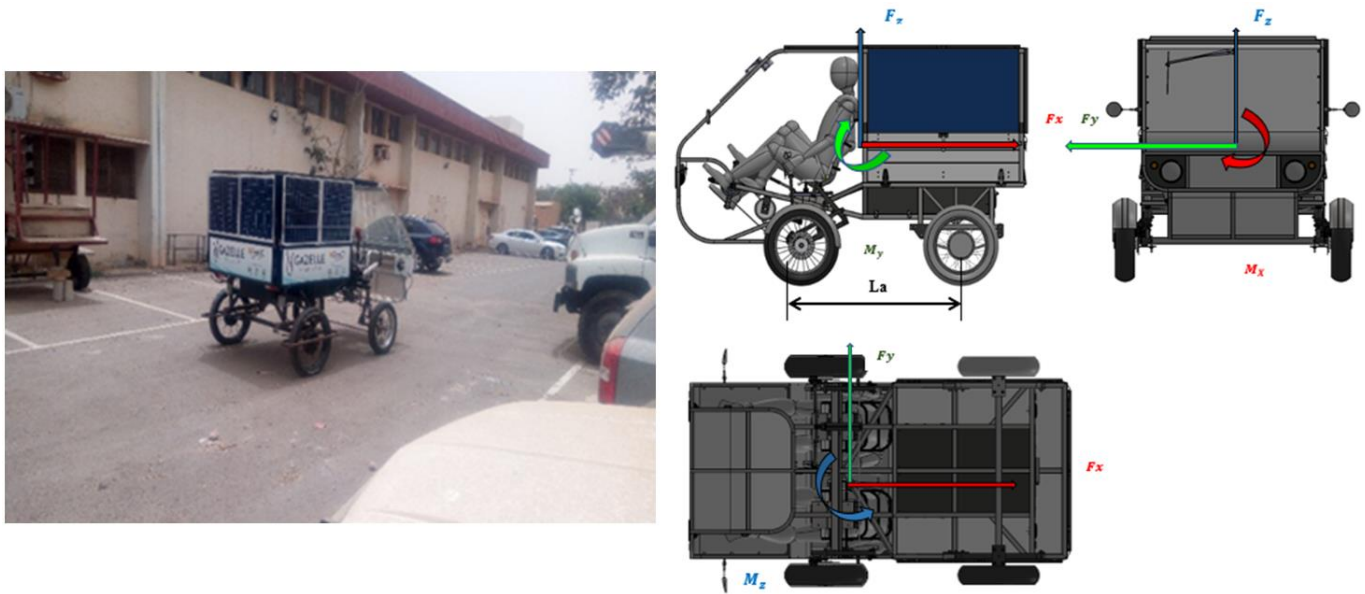
Fig. 2.   Aerodynamic Torsor

3   METHODOLOGY

The environment and driving conditions [21] can also affect aerodynamics, including factors such as

- The profile of the trajectory;
- wheel rotation;
- Climatic conditions like rain and wind;
- Considerations for reducing rolling resistance include the type of road surface, ground clearance, load impact;
- tyre selection;
- vehicle shape.

Consistency in these factors can lead to improved efficiency and reduced energy consumption.

3.1   CLASSICAL APPROACH

The wind tunnels facilitate the analysis of aerodynamic factors with high repeatability and under specific conditions, following a comprehensive investigation of the aerodynamic torser in stable airflow. Wind tunnels are tailored to predetermined specifications for aerodynamic analysis, allowing for reliable and repeatable analysis in a controlled environment. These tunnels allow for the observation of flow following the shape of the bodywork under limited conditions, based on a thorough study of the aerodynamic torsor under steady airflow.

The use of Open Circuit Suction Wind Tunnels (OCSWT) is generally preferred for analyzing aerodynamic factors with repeatability and under specific conditions [22]. These tunnels allow for the observation of flow following the shape of the bodywork under limited conditions, based on a thorough study of the aerodynamic torsor under steady airflow.

Engineers construct various models and quantitatively evaluate them to determine their global measurable quantities, such as aerodynamic torsion. The study has chosen the optimal design after considering past methods, which included smoke and statistical pressure measurements [23], but were limited. The flow exhibited deficiencies, and comprehension of the correlations between shape and flow, as well as the global and local flow structure, was unclear.

3.2   CALCULATION AND TESTING APPROACH

Advancements in aerodynamics research have led to improved techniques for measuring and analyzing the interactions between shapes and flow, resulting in more accurate model validations [24]. Reliable and rapid calculations can now determine aerodynamic quantities. Additionally, the development of simulation and calculation software has made it possible to obtain

ideal global values of the aerodynamic torsor, replacing the need for physical testing. However, it is often necessary to compare numerical simulation and testing to obtain combined results [9].

Another advantage of using the numerical method is having the flexibility to use sufficient boundary conditions, which is limited in the wind tunnel method [25].

The improved Delayed Detached-Eddy Simulation (IDDES) [24] is a simulation method typically utilized to determine the aerodynamic performance of high-speed trains [26]. A reduced ground clearance is shown to lower the aerodynamic drag of the front end [27].

The K-epsilon model (K-Ɛ) is a simulation for turbulent flow characteristics [28].

4 SIMULATION AND RESULT OF THE AERODYNAMIC STUDY OF THE MOBILE GENERATOR

4.1 GEOMETRY MODEL

As illustrated in Figure 4, the generator comprises of a cab and a body. The generator has no doors or windows in the cab, promoting the internal circulation of air within the body. Its dimensions are 1886.6 mm in height, 2948.04 mm in length, and 1970 mm in width. The digital model will be used for simulation and the geometry conforms to the technical requirements of the computer mesh. The generator has no doors or windows in the cab, promoting the internal circulation of air within the body. The body is enclosed on two sides and a rear side. The wheelbase measures 1340.98 mm, crucial for determining the moment between the front and rear wheels. The generator's ground clearance is 317.5 mm. Figure 4 illustrates the generator's characteristic lengths. The profile plays a significant part in the aerodynamic study [29]. To increase efficiency, the generator is engineered to balance the energy production capacity of the photovoltaic cells with the aerodynamic performance [30].The mesh is produced according to its dimensions [31].

Fig. 3.   Gazelle Generator
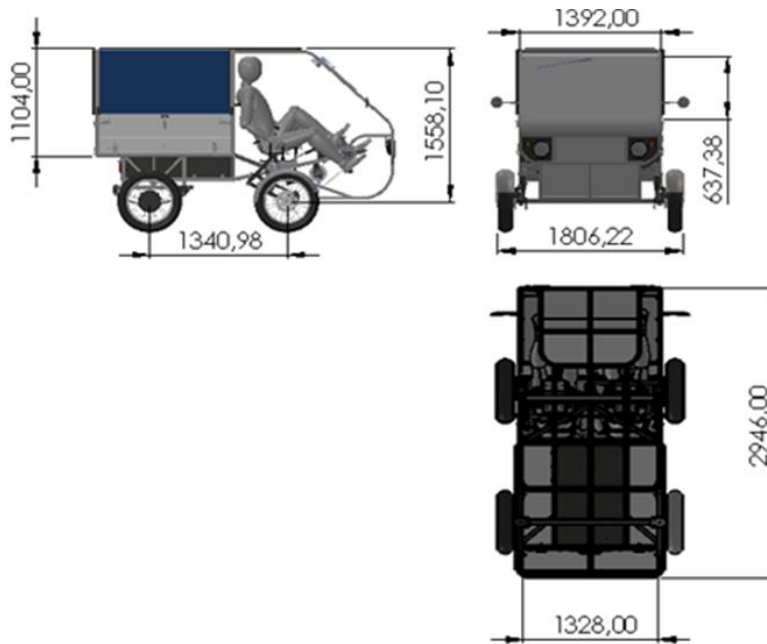
Fig. 4.   Characteristic lengths of the generator

4.2   ANALYTICAL METHOD FOR DETERMINING THE AERODYNAMIC RESISTANCE

The formula for aerodynamic drag is given by the following equation:

$$R_a = \frac{1}{2} \times \alpha \times C_x \times S \times v^2 \quad (10)$$

It is believed that the drag appears as shape drag, specifically a frontal impact [32], [33] of a cubic shape, resulting in a value of Cx = 0.8 (refer to Figure 1). The tables below contain the values of aerodynamic constant parameters.

Table 1. Characteristic lengths of the generator

Height *(mm)*	Width *(mm)*	Length *(mm)*	Coefficient *(mm)*	Frontal area *(mm²)*
1886,6	1970	2948,04	0,81	3,010

The air density α is 1.225 kg/m3, the drag coefficient is 0.8

$$0.5 \times 1{,}225 = 0{,}61 \quad (11)$$

$$\frac{1}{1{,}6} = \frac{10}{16} \quad (12)$$

$$R_a = \frac{10 \times C_x \times S \times v^2}{16} \quad (13)$$

$\frac{C_x \times S}{16}$ Represents the shape coefficient

$\frac{1}{2} \times \alpha \times v^2$ Is the dynamic pressure

In the simulation, we determined the value of the shape coefficient and the dynamic pressure and saw their variations as a function of the variation in speed. The parameters considered are given in the following table:

Table 2. Parameters considered Ra value

Velocity *(m/s)*	Dynamic pressure *(Pa)*	Air resistance *(N)*
4,17	10,63	25,61
5	15,31	36,88
5,83	20,84	50,20
6,66	27,22	65,56
7,50	34,45	82,98
8,33	42,54	102,44
9,17	51,47	123,95
9,72	57,90	139,43
9,91	60,23	145,06

The aerodynamic drag value is 145.064 N at maximum speed.

$$R_{a.max\ anal.} = 145,064\ N$$

The variation curves are given by:
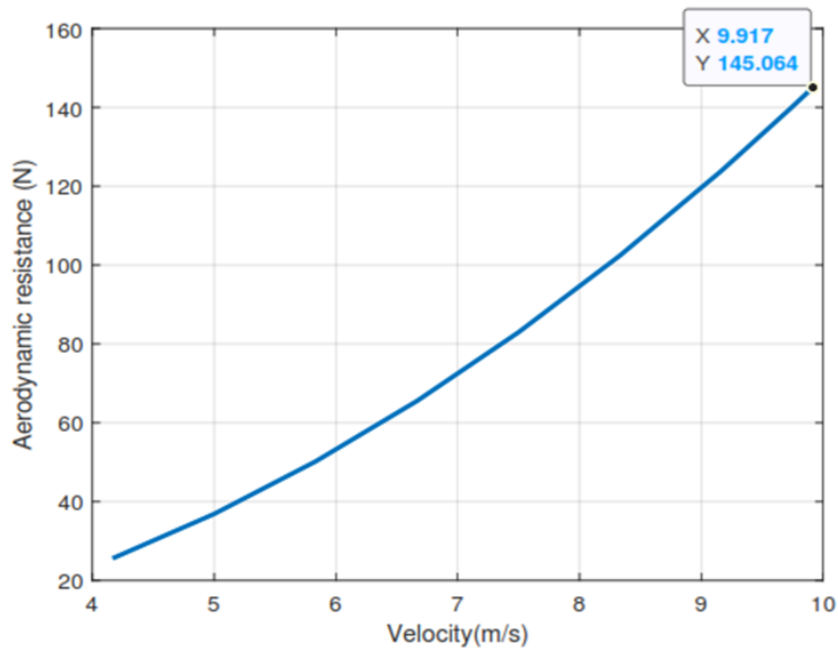
Fig. 5.   Variation of Aerodynamic
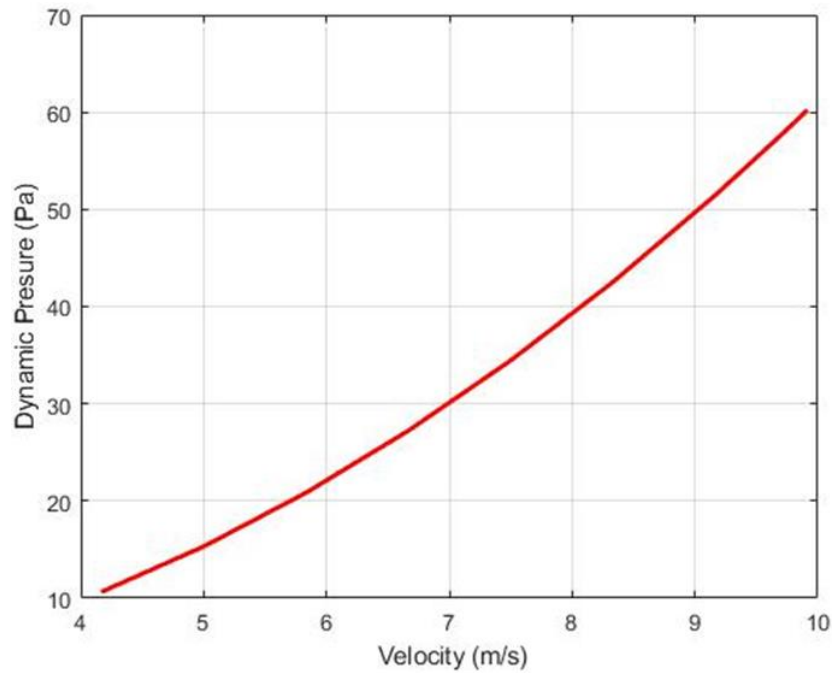
Fig. 6.   Variation of Dynamic pressure

4.3   NUMERICAL METHOD

In this work, numerical simulations were performed with SolidWorks software for the determination of the aerodynamic force and dynamic pressure. The ANSYS Fluent software is also used for the value of the drag along the profile of the generator shape. It also gives the airflow pattern on the side and rear faces of the generator, and especially on the master torque. In the tuning parameters, second degree wind patterns are used for the discretization of the terms [34].An iteration number of 100 was applied. The chosen speed is 9.917 m/s corresponding to the maximum speed of the generator, i.e., 35.7 km per hour.
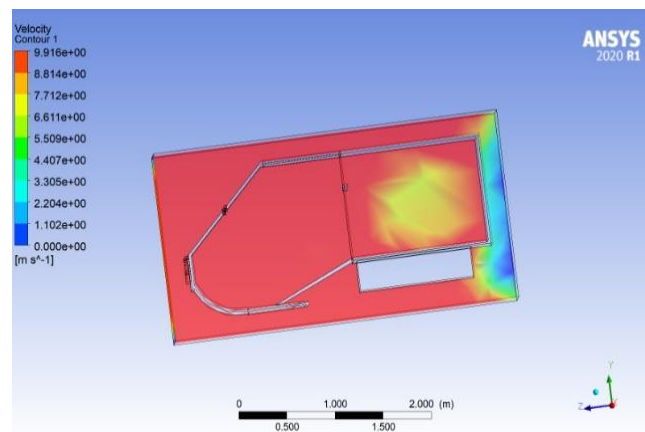
Fig. 7.   Variation in internal pressure

GG Force normale (Z) 2	139.391 N	Atteinte (IT = 41)	37.5456 N	138.928 N
GG Moyenne Pression dynamique 1	64.1641 Pa	Atteinte (IT = 139)	0.180233 Pa	64.1524 Pa
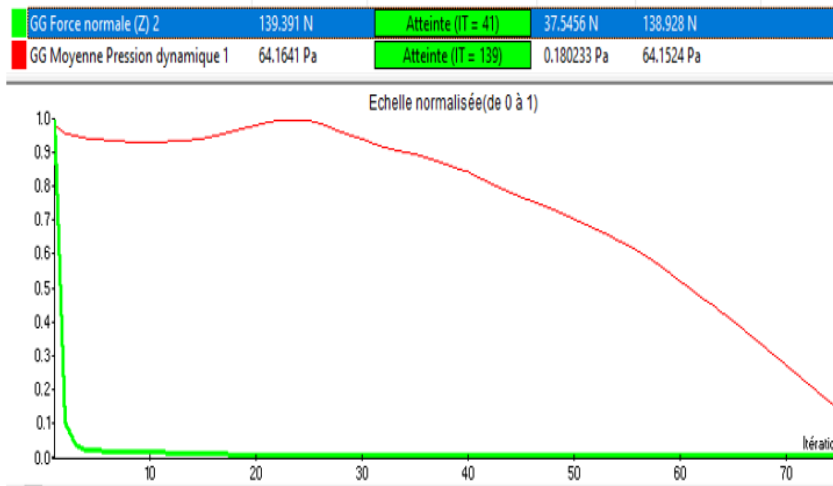
Fig. 8.   Aerodynamic force and dynamic pressure
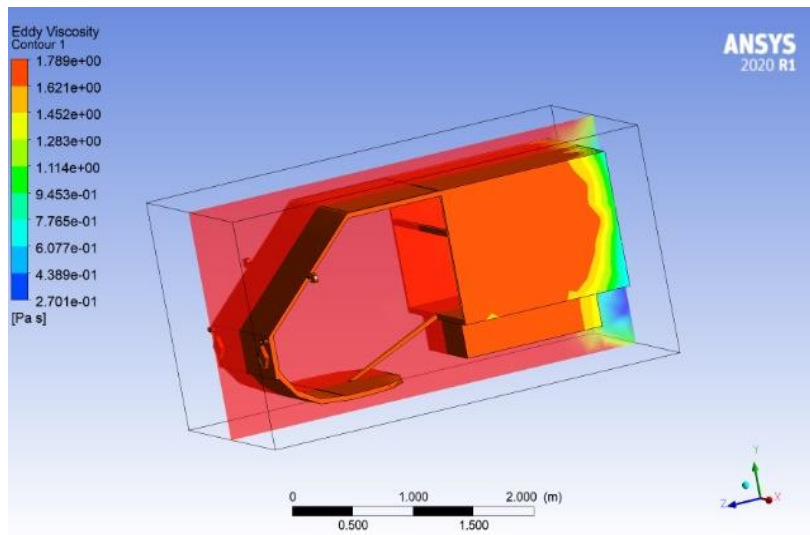
Fig. 9.   Zones of turbulence
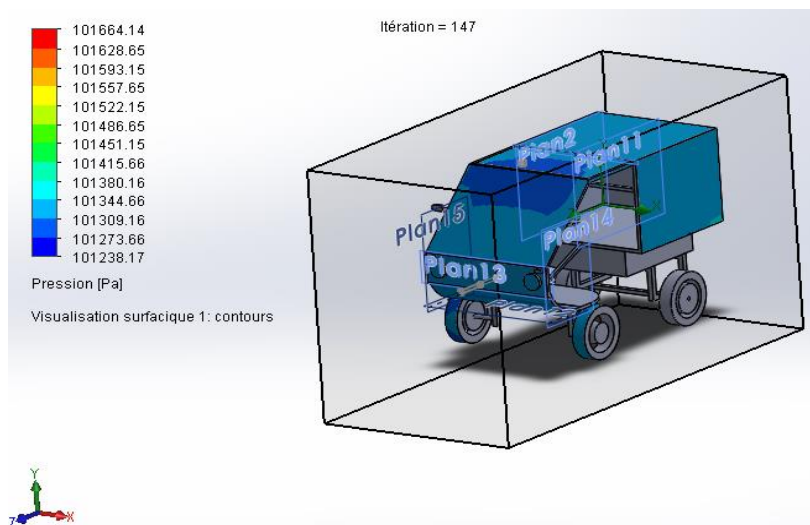
Fig. 10.   Surface visualisation
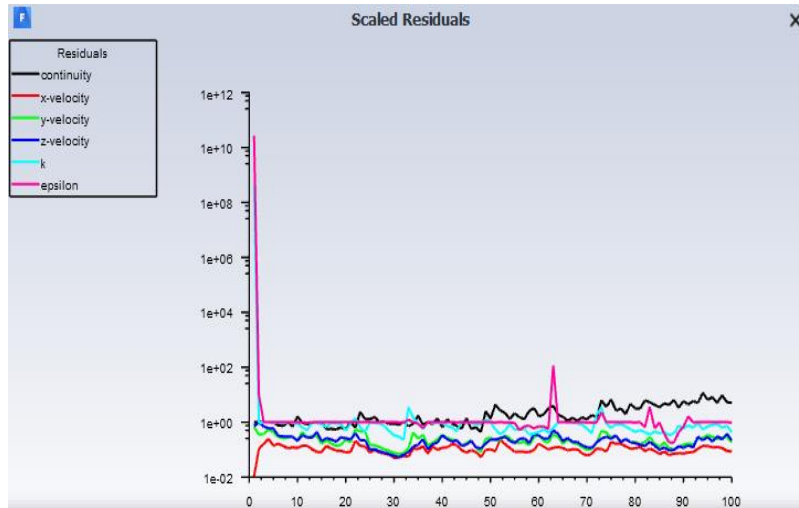
Fig. 11.   Drag profile with the K-epsilon method
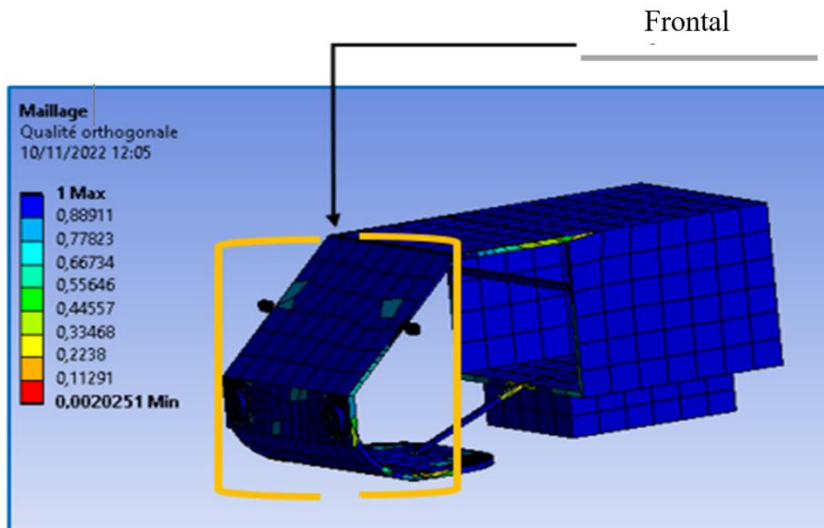
Fig. 12.   Networking
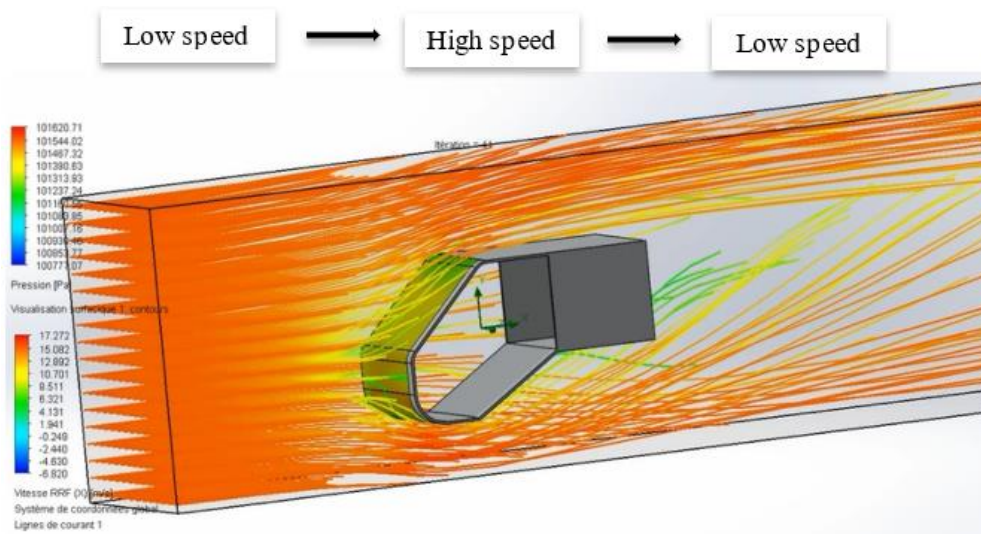
Fig. 13.   Flow pattern according to the shape

5 CALCULATION OF DISSIPATED POWER

At zero gradient, i.e., on a level road and at maximum speed, the power transmitted to the wheels is dissipated by aerodynamic drag and rolling resistance [35].
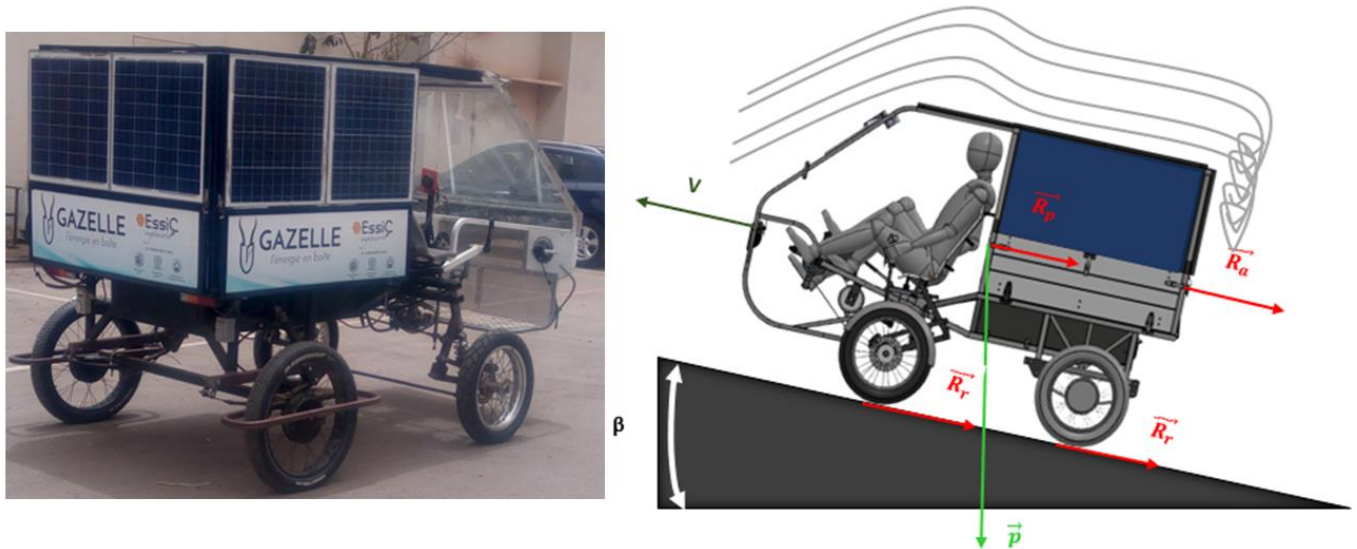
Fig. 14. *Forces to overcome*

$$P_m = \frac{1}{\eta} \times v \times (R_a + R_r + R_p)$$

$$P_m = \frac{1}{1000 \times \eta \times 3,6} \times (M \times K \times V$$

With K: tensile strength coefficient, also known as the tensile strength determined by the Andreau formula [36]:

$$K = 10 \left(\frac{20}{\rho^{0.64}} + \frac{v^{3.7}}{1294000 \times \rho^{2.08}}\right) \quad (16)$$

$$P_m = \frac{1}{1000 \times \eta} \times v \times \left(M \times K + \frac{10 \times C_x \times S \times v^2}{16}\right) \quad (17)$$

Table 3. *Calculated power output*

Velocity *(m/s)*	Air resistance *(N)*	Power (W)
4.17	25.61	106.7
5	36.88	184.39
5.83	50.20	292.80
6.66	65.56	437.07
7.50	82.98	622.31
8.33	102.44	853.66
9.17	123.95	1136.21
9.72	139.43	1355.57
9.91	145.06	1438.55
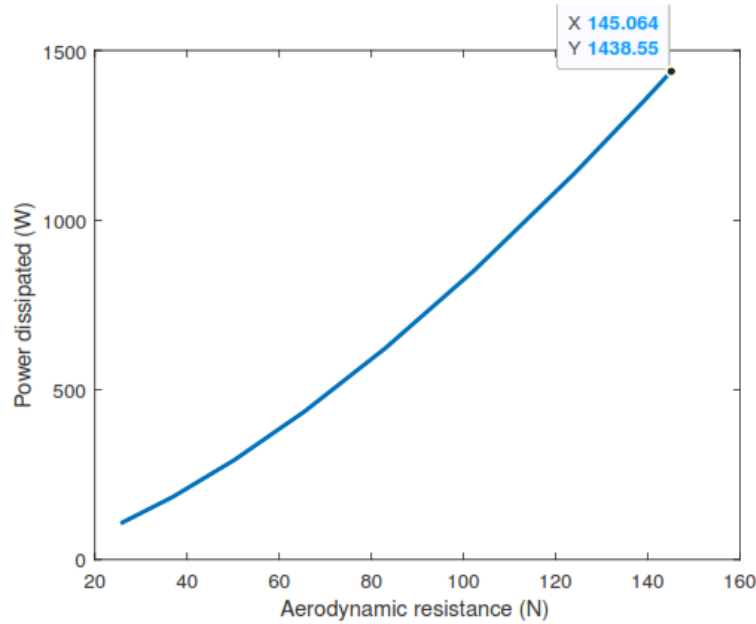
Fig. 15.   Variation of the power dissipated by the aerodynamics

6   DISCUSSION

The curves generated from the analytical method demonstrate that as the speed variation increases, the aerodynamic resistance gains more significance. For each constant increase in speed by 0.834 m/s, the aerodynamics displays a proportional increase with an average value of 17.34 N. This change causes an upsurge in dynamic parameters, including dynamic pressure P_d. At the maximum speed, the resistance reaches a maximum value of 145.064 N. This is due to the increasing significance of the air impact force as speed increases. The air acts as a resistance to the forward motion of the mobile generator. The dynamic pressure is measured at 60.233 Pa.

At the maximum speed, the numerical method yields a maximum resistance of 138.40 N, while the analytical method's resistance varies with speed. Upon initial exposure to the air, low lift generates significant drag, which in turn creates high pressure. The shock effect is mitigated by the generator's geometry, particularly on the rounded sections, resulting in an average value of low pressure at 133.147 N. This value is explained by the large surface area perpendicular to the air field lines, resulting in a higher pressure at 101664.14 Pa. The resulting dynamic pressure is 64.1641 Pa.

COMPARISON OF BOTH METHODS

The analytical method gives a value of resistance at maximum speed (V max =37.5 km/h) of 145.06 N, and that given by the numérique is 138.391 N so the difference found is:

$$\Delta R_{amax} = \frac{145.064 - 138.391}{145.064} \ X \ 100 = 4.22 \ \%$$

Aerodynamics has a consequence on the performance by influencing the power of the generator and the stability i.e., the handling [23] of the generator. We will check the influence of aerodynamics on the power of the generator.

For the dynamic pressure we have:

$$P_d = \frac{1}{2} \times \alpha \times \ v^2$$

$$P_d = \frac{1}{2} \times 1.22 \times 9.917^2$$

$$P_d = 60.233 \ Pa$$

The numerical calculation gives 64.1641 Pa

$$\Delta P_{d.max} = \frac{64.1641 - 60.233}{64.152} \times 100 = 6.1\%$$

As depicted in *Fig. 8,* the pressure above the airfoil is marginally lower than below, producing a relatively modest lift force. The foremost source of aerodynamic drag can be attributed to the pressure line visible on the leading edge as depicted in the figure.

With the exception of the generator's frontal surface and lower part of its windscreen, the entire generator body exhibits low pressure. This low-pressure phenomenon is centered around the curved edges, where the air is disrupted.

The flow occurs in two areas of the generator: an internal flow (*Fig. 7*) and a flow over the body's shape. *Fig. 9* and *Fig. 11* demonstrate a sudden change in the flow along the generator's profile.

We can infer that a high-pressure zone exists on the front face whilst a turbulence zone arises towards the rear of the generator due to its shape, which generates drag.

The generator's front face experiences air pressure, demonstrated in the figure, resulting in shape drag as indicated by pressure variation curves aligned with directions. The pressure representation confirms the presence of turbulence trail. Air flow produces frictional drag particularly over the roof of the generator while passing over its body. Turbulence occurs towards the rear of the generator, specifically the upper part of the rear side, as illustrated in figures 7 and 11. As the generator lacks side doors, air flows inside, causing internal turbulence due to trapped air, resulting in internal drag.

The graph depicted in Figure 5 illustrates the significant impact of aerodynamics on power dissipation. At the initial speed of 18 km/h, the air resistance measures at 25.61 N, with a corresponding power dissipation of 106.707 W. As air resistance increases, so does the power dissipated, increasing at a far greater rate than that of aerodynamics. At maximum speed of 35.7 km/h, power dissipation skyrockets to 1438.55 W, with air resistance measuring at 145.064 N. Therefore, it is evident that aerodynamics plays a paramount role in the dissipation of power. The power output is indirectly dependent on the weight of the generator, which is linked to rolling resistance. The findings reveal that minimal variations in speed cause significant differences in power output, owing to aerodynamics since air resistance is proportional to the square of speed.

Consequently, it can be inferred that when in motion, a dissimilarity in power output is brought about by aerodynamics between two velocities. This disparity is equivalent to the difference of squares of said velocities.

$$R_{a2} - R_{a1} = \frac{1}{2} \times \alpha \times C_x \times S \times v_2^2 - \frac{1}{2} \times \alpha \times C_x \times S \times v_1^2 = \frac{1}{2} \times \alpha \times C_x \times S \times A\,(v_1^2 - v_2^2) \quad (18)$$

$$\Delta Ra = A \times (v_1^2 - v_2^2) \quad (19)$$

$$A = \frac{1}{2} \times \alpha \times C_x \times S = \frac{1}{2} \times 1,225 \times 0,8 \times 3.010 = 1.4749$$

A is the aerodynamic constant

Since the difference only affects the speed which varies then, For the squares of the Speed, their difference shows that air resistance dissipates power:

$$\Delta V = (v_2^2 - v_1^2)^{\frac{1}{2}} \quad (20)$$

Between speeds of 15 and 18 km/h we have the table 4:

$$\Delta V = (v_2^2 - v_1^2)^{\frac{1}{2}} \quad \Delta V = (18^2 - 15^2)^{1/2} = 9{,}95 \text{ km/s}$$

This means that between 15 and 18 km/h, in order to maintain a speed of 18 instead of 15 km/h, the power dissipated by the air resistance at the speed of 9.95 km/h is required and in the opposite case the same energy consumption is recovered by going from 18 to 15 km/h.

$$P_m = \frac{1}{0{,}85} \times 2,76 \times \left(1.4749 \times 2.76^2\right)$$

$$P_m = 36.48 \ W$$

Table 4.   Variation in dissipated power with increasing speed

Speed Passage	ΔV (km/h)	ΔV (m/s)	Power dissipated (W)	ΔP (W)
15-18	9.95	2.76	36.48	0
18-21	10.82	3.00	47.07	11.27
21-24	11.62	3.23	58.34	12.05
24-27	12.37	3.44	70.38	12.78
27-30	13.08	3.63	83.16	13.47
30-33	13.75	3.82	96.63	14.13
33-36	14.39	4.00	110.76	14.76
35-35,7	15.00	4.17	125.52	14.76

So, increasing the speed from 15 to 18 km/h leads to a power dissipation of 36.48 W due to rolling resistance.

Moreover, moving a vehicle through the air necessitates power that grows with the cube of the speed.

Table 5.   Impact of speed change on power dissipated by aerodynamics

39	36.00	34.60	32.86	30.74	28.14	24.92	20.78	17.20	0.00
36	32.73	31.18	29.24	26.83	23.81	19.90	14.39	0.00	15.00
33	29.39	27.66	25.46	22.65	18.97	13.75	0.00	14.39	13.62
30	25.98	24.00	21.42	18.00	13.08	0.00	13.75	18.03	19.35
27	22.45	20.12	16.97	12.37	0.00	13.08	18.97	22.27	23.36
24	18.73	15.87	11.62	0.00	12.37	18.00	22.65	25.48	26.43
21	14.70	10.82	0.00	11.62	16.97	21.42	25.46	28.00	28.87
18	9.95	0.00	10.82	15.87	20.12	24.00	27.66	30.02	30.83
15	0.00	9.95	14.70	18.73	22.45	25.98	29.39	31.62	32.40
Speed in km/h	**15**	**18**	**21**	**24**	**27**	**30**	**33**	**35**	**35.7**

To increase from a velocity of 18 to 21 km/h, there must be a rise in speed of 3 km/h, as indicated in the table. This rise gives rise to a difference of 10.82 km/h, and therefore results in an air resistance power dissipation of 11.27 W at this particular speed. In order to attain a velocity of 24 km/h, a difference of 11.62 km/h is required, resulting in a power dissipation of 12.05 W. The average power, in light of all the velocities considered, is 12.69 W. This means that:

$$24 \ km/h = 15 \ km + 9.95 \ km + 10.82 \ km + 11.62$$

$$24^2 = 15^2 + 9.95^2 + 10.82^2 + 11.62^2 = 576$$
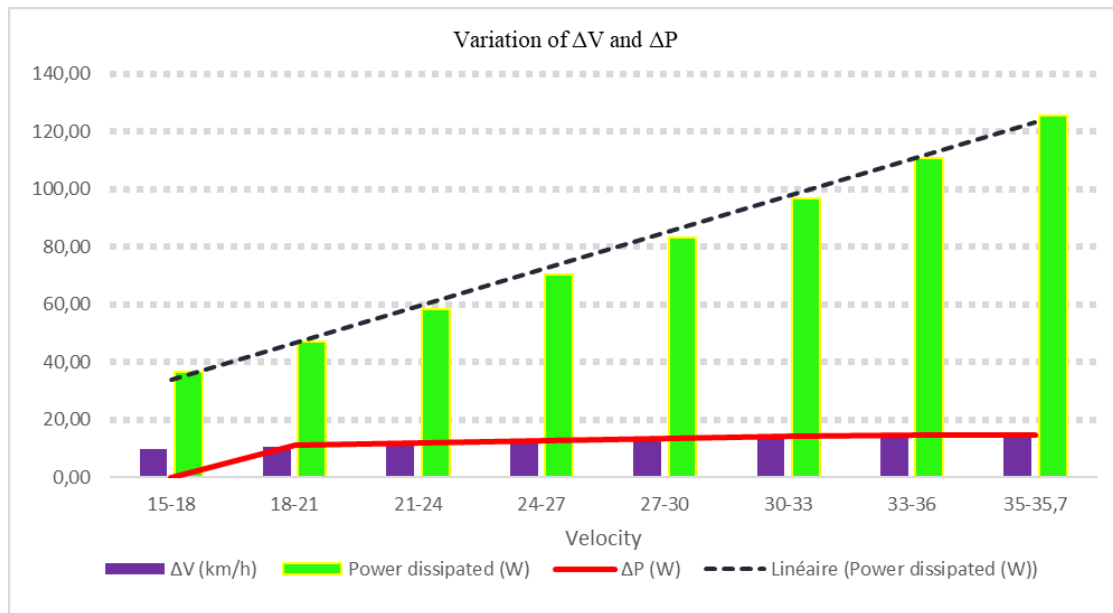
Fig. 16.   Variation of ΔV and ΔP

Fig. 16 shows that a small difference in speed leads to a significant increase in the power dissipated. This confirms that for the generator, a speed change of 3 km/h generates an average power dissipation of 12.69 W. The curve linking the peaks representing power shows us that this increase is linear.

7   CONCLUSION

We have uncovered an issue with the generator's aerodynamic drag. Our investigation has shown that the photovoltaic generator faces resistance from both air and rolling when in motion, resulting in a loss of power. Aerodynamics make a significant contribution to these forces. Air resistance, which rises proportionally with the square of velocity, encounters a noteworthy peak when cruising at 9.916 m/s. Air resistance results in an increase of 1438.55 W in power dissipation caused by 145.064 N. Additionally, alterations in speed require extra power consumption. The aerodynamic behaviours were analysed through the utilisation of SOLIDWORKS and ANSYS modelling software, and the relevant parameter variation curves were plotted using MATLAB. For global analysis of the complex aerodynamic forces and moments that affect the generator, a three-dimensional flow model was adopted to enhance the simulation performance.

REFERENCES

[1]   S. M. Rakibul Hassan, T. Islam, M. Ali, and M. Q. Islam, «Numerical study on aerodynamic drag reduction of racing cars,» in *Procedia Engineering,* Elsevier Ltd, 2014, pp. 308–313. doi: 10.1016/j.proeng.2014.11.854.

[2]   E. Orlik, «Etude du champ aérodynamique et de la transition laminaire-turbulent sur l'avant-corps d'un véhicule hypersonique.» [Online]. Available: https://tel.archives-ouvertes.fr/tel-00573692.

[3]   J.-L. Aider, L. Elena, Y. Le Sant, and F. Bouvier, «Aérodynamique automobile Marie-Claire Merienne et Jean-Luc Peron ONERA,» 2018. [Online]. Available: www.onlinedoctranslator.com

[4]   D. Singla, A. Tayal, R. Sharma, and J. P. Kesari, «Aerodynamic Development of a Solar Car.» [Online]. Available: www.ijert.org

[5]   J. P. Pauwelussen, «Fundamentals of Tire Behavior,» in *Essentials of Vehicle Dynamics,* Elsevier, 2015, pp. 7–74. doi: 10.1016/b978-0-08-100036-6.00002-9.

[6] G. Sivaraj, K. M. Parammasivam, M. S. Prasath, P. Vadivelu, and D. Lakshmanan, «Low analysis of rear end body shape of the vehicle for better aerodynamic performance,» in *Materials Today: Proceedings,* Elsevier Ltd, 2021, pp. 2175–2181. doi: 10.1016/j.matpr.2021.05.521.

[7] J. Katz, «Aerodynamics of Race Cars,» 2005, doi: 10.1146/annurev.fluid.

[8] J. P. Pauwelussen, «Fundamentals of Tire Behavior,» *Essentials Veh. Dyn.,* pp. 7–74, Jan. 2015, doi: 10.1016/B978-0-08-100036-6.00002-9.

[9] L. Elena and X. Bohineust, «COMPLEMENTARITE CALCULS / ESSAIS EN AERODYNAMIQUE AUTOMOBILE.».

[10] A. Kocoń and A. Flaga, «Critical velocity measurements of freight railway vehicles roll-over in wind tunnel tests as the method to assess their safety at strong cross winds,» *J. Wind Eng. Ind. Aerodyn.,* vol. 211, p. 104559, Apr. 2021, doi: 10.1016/J.JWEIA.2021.104559.

[11] T. Ren, Z. Zhu, J. Wang, and C. Yan, «Numerical simulation of flow resistance characteristics in a rod bundle channel under rolling conditions,» *Ann. Nucl. Energy,* vol. 181, p. 109573, Feb. 2023, doi: 10.1016/J.ANUCENE.2022.109573.

[12] V. I. Smirnov and S. A. Vidyushenkov, «Air Resistance of Rolling Wagons on the Marshalling Hump,» *Transp. Res. Procedia,* vol. 68, pp. 294–302, Jan. 2023, doi: 10.1016/J.TRPRO.2023.02.040.

[13] B. Wang, W. Wang, Y. Li, and F. Lan, «Aerodynamic characteristics study of vehicle-bridge system based on computational fluid dynamics,» *J. Wind Eng. Ind. Aerodyn.,* vol. 234, p. 105351, Mar. 2023, doi: 10.1016/J.JWEIA.2023.105351.

[14] J. Niu, D. Zhou, and X. Liang, «Numerical investigation of the aerodynamic characteristics of high-speed trains of different lengths under crosswind with or without windbreaks,» *Eng. Appl. Comput. Fluid Mech.,* vol. 12, no. 1, pp. 195–215, Jan. 2018, doi: 10.1080/19942060.2017.1390786.

[15] V. Kumar Singh, S. Marwaha, and A. Kumar Singh, «Design and Analysis of Permanent Magnet Brushless DC Motor for Solar Vehicle using Ansys Software.» [Online]. Available: www.ijert.org

[16] Z. Ma, Z. Liu, H. Zou, and J. Liu, «Dynamic modeling and analysis of satellite detumbling using a brush type contactor based on flexible multibody dynamics,» *Mech. Mach. Theory,* vol. 170, Apr. 2022, doi: 10.1016/j.mechmachtheory.2021.104675.

[17] H. Ustarroz *et al.,* «ETUDE AERODYNAMIQUE M1C2PA-Yvain SUBRA Travail présenté par.».

[18] C. Baker, Train aerodynamics : fundamentals and applications.

[19] J. Y. Zhu and Z. W. Hu, «Flow between the train underbody and trackbed around the bogie area and its impact on ballast flight,» *J. Wind Eng. Ind. Aerodyn.,* vol. 166, pp. 20–28, Jul. 2017, doi: 10.1016/J.JWEIA.2017.03.009.

[20] Society of Automotive Engineers., Emissions : advanced catalyst and substrates, measurement and testing, and diesel gaseous emissions. SAE International, 2003.

[21] J.-L. Aider, L. Elena, Y. Le Sant, F. Bouvier, M.-C. Merienne, and J.-L. Peron, «Pressure-Sensitive Paint for Automotive Aerodynamics,» 2001.

[22] B. Celis and H. H. Ubbens, «Design and Construction of an Open-circuit Wind Tunnel with Specific Measurement Equipment for Cycling,» in *Procedia Engineering,* Elsevier Ltd, 2016, pp. 98–103. doi: 10.1016/j.proeng.2016.06.196.

[23] H. Hemida, «Contribution of computational wind engineering in train aerodynamics—past and future,» *J. Wind Eng. Ind. Aerodyn.,* vol. 234, p. 105352, Mar. 2023, doi: 10.1016/J.JWEIA.2023.105352.

[24] Z. Guo, T. Liu, Y. Xia, and Z. Liu, «Aerodynamic influence of the clearance under the cowcatcher of a high-speed train,» *J. Wind Eng. Ind. Aerodyn.,* vol. 220, Jan. 2022, doi: 10.1016/j.jweia.2021.104844.

[25] H. Chowdhury, B. Loganathan, I. Mustary, H. Moria, and F. Alam, «Effect of Various Deflectors on Drag Reduction for Trucks,» in *Energy Procedia,* Elsevier Ltd, 2017, pp. 561–566. doi: 10.1016/j.egypro.2017.03.185.

[26] H. Kwon, «A study on the resistance force and the aerodynamic drag of Korean high-speed trains,» *Veh. Syst. Dyn.,* vol. 56, no. 8, pp. 1250–1268, Aug. 2018, doi: 10.1080/00423114.2017.1410184.

[27] H. Ozawa, S. Nishikawa, and D. Higashida, «Development of aerodynamics for a solar race car,» 1998.

[28] T. B. Korkut and A. Gören, «Aerodynamic effect of wing mirror usage on the solaris 7 solar car and demobil 09 electric vehicle,» *Int. J. Automot. Mech. Eng.,* vol. 17, no. 2, pp. 7868–7881, Apr. 2020, doi: 10.15282/ijame.17.2.2020.06.0587.

[29] H. Kozmar, K. Butler, and A. Kareem, «Transient cross-wind aerodynamic loads on a generic vehicle due to bora gusts,» *J. Wind Eng. Ind. Aerodyn.,* vol. 111, pp. 73–84, 2012, doi: 10.1016/j.jweia.2012.09.001.

[30] H. Heisler, «Vehicle body aerodynamics,» *Adv. Veh. Technol.,* pp. 584–634, Jan. 2002, doi: 10.1016/B978-075065131-8/50015-4.

[31] N. E. Ahmad, Abo-Serie, and Gaylard, «Mesh optimization for ground vehicle Aerodynamics,» *CFD Lett.,* vol. 2, no. 1, pp. 54–65, 2009, [Online]. Available: www.cfdl.issres.net

[32] U. Faculté De, «République Ministère de L'Enseignement Mémoire de Fin d'Etude de MASTER ACADEMIQUE Modélisation et simulation sous MATALAB/SIMULINK d' photovoltaïque adapté Mr Nabil BENYAHIA Mr Mustapha ZAOUIA Mr Hakim DENOUN Mr Hakim DJOUDI.».

[33] E. S. Aziz, C. Chassapis, S. Esche, S. Dai, S. Xu, and R. Jia, «Online wind tunnel laboratory,» in *ASEE Annual Conference and Exposition, Conference Proceedings,* American Society for Engineering Education, 2008. doi: 10.18260/1-2--3402.

[34] D. Flynn, H. Hemida, D. Soper, and C. Baker, «Detached-eddy simulation of the slipstream of an operational freight train,» *J. Wind Eng. Ind. Aerodyn.,* vol. 132, pp. 1–12, Sep. 2014, doi: 10.1016/J.JWEIA.2014.06.016.

[35] S. Kang, H. Ozer, I. L. Al-Qadi, and B. F. Spencer, «Stochastic Analysis of Rolling Resistance Energy Dissipation for a Tractor-Trailer Model,» *Transp. Res. Rec.,* 2019, doi: 10.1177/0361198119840344.

[36] «RÉFLEXIONS SUR L' ÉNERGÉTIQUE DES VÉHICULES ROUTIERS.».